Pergamon

Geochimica et Cosmochimica Acta, Vol. 68, No. 20, pp. 4201-4211, 2004

0016-7037/04 $30.00 + .00

doi:10.1016/j.gca.2004.04.013

Si in the core? New high-pressure and high-temperature experimental data

VALÉRIE MALAVERGNE,[1,*] JULIEN SIEBERT,[1,2] FRANÇOIS GUYOT,[2,3] LAURENT GAUTRON,[1] ROSSANA COMBES,[1] TAHAR HAMMOUDA,[4] STEPHAN BORENSZTAJN,[5] DAN FROST,[6] and ISABELLE MARTINEZ[7]

[1]Université de Marne-La-Vallée, Laboratoire des Géomatériaux and FRE CNRS 2455, Cité Descartes, Champs-sur-Marne, 77454 Marne-La-Vallée Cédex, France
[2]Institut de Physique du Globe de Paris, 4 place Jussieu, 75 252 Paris cedex 05, France
[3]Laboratoire de minéralogie-cristallographie and UMR CNRS 7590, Case 115, 4 place Jussieu, 75 252 Paris cedex 05, France
[4]Laboratoire Magma et Volcan, OPGC, Université Blaise Pascal—CNRS, 5 rue Kessler, 63038 Clermont-Ferrand cedex, France
[5]UPR15 du CNRS, Physique des Liquides et Electrochimie, 4 Place Jussieu, 75252 Paris Cedex 05, France
[6]Bayerisches Geoinstitut, Universität Bayreuth, D-95440, Bayreuth, Germany
[7]Laboratoire de Géochimie des Isotopes Stables, IPGP—Université Paris 7, 2, place Jussieu, Tour 54-64 -75252 Paris Cedex 05, France

(*Received* June 2, 2003; *accepted in revised form* April 7, 2004)

Abstract—High-pressure high-temperature experiments have been carried out up to 25 GPa and 2200°C in a multianvil press on assemblages made of silicates and iron-silicon alloys. At 20 GPa, silicon is extracted from the metal phase, forming stishovite reaction rims around metal grains. The silicon content in metal has been measured by analytical electron microscopy and electron microprobe. In contrast with earlier experiments, the present data were obtained by using silicon-rich metal alloys as starting materials instead of studying incorporation of silicon in initially silicon-free metal. As in most of previous studies carried out below 25 GPa, the silicon content in liquid metal increases with increasing pressure and with decreasing oxygen fugacity. The oxygen fugacity in most experiments was calculated by using two independent buffers: iron/wüstite (IW) and SiO_2/Si, allowing to link consistently the Fe contents in silicates, the Si contents in metal and the temperatures of the experiments. At oxygen fugacities 4 log units below IW, silicates are in equilibrium with Si-rich metallic alloys (up to 17 wt% of Si in metal at 20 GPa and 2200°C). Extrapolation to 2 log units below IW leads to less than 0.1 wt% Si in the metal phase. Presence of several wt% of silicon in the Earth's core thus requires highly reduced initial materials that, if equilibrated at conditions relevant to small planets, should already contain significant amount of silicon dissolved in metal.

1. INTRODUCTION

High-pressure and high-temperature metal-silicate interactions play a role in establishing the composition of the Earth's core. Within the framework of a given scenario for core segregation, high-pressure partitioning of elements between metal and silicate constrains the nature of the light elements present in the core (e.g., Ringwood, 1984; Knittle and Jeanloz, 1989; Goarant et al., 1992; Poirier, 1994).

In agreement with some geochemical studies (e.g., Wänke et al., 1984; Ringwood, 1979; Allègre et al., 1995, 2001; Javoy, 1995), several experimental studies suggest that silicon could be an important light element in the Earth's core. The process of silicon incorporation is:

$$2Fe_{metal} + SiO_{2silicate} \leftrightarrow 2FeO_{silicate} + Si_{metal} \quad (1)$$

If reaction 1 proceeded to the right at conditions prevailing during core segregation, it is possible that significant amounts of Si could have been incorporated into the core. Ito and Katsura (1991) and Ito et al. (1995) showed that high-pressure, high-temperature reaction between $MgSiO_3$ and pure iron at 26 GPa and 2500°C resulted in up to 2 wt% of Si in the metal phase. Moreover, the presence of FeO observed by Ito and Katsura (1991) and Ito et al. (1995) in contact with grains of metal is consistent with reaction 1. These results have been corroborated by Othani et al. (1997), O'Neill et al. (1998), and Gessmann and Rubie (1998).

The importance of fO_2 on Si solubility in metal has been confirmed by Kilburn and Wood (1997) and Li and Agee (2001b). Similarly, Javoy (1995), Guyot et al. (1997), Gessmann and Rubie (1998), and Gessmann et al. (2001) suggested that several wt% Si could be incorporated in metal according to reaction 1 at high temperature and at pressures between 5 and 20 GPa, under more reducing conditions than the present redox state of the mantle. Such silicon incorporation, however, is impossible at higher pressure as suggested by Javoy (1995) and O'Neill et al. (1998) and by the experimental results of Hillgren and Boehler (1998, 1999) and Dubrovinsky et al. (2003), in agreement with the model of Guyot et al. (1997). The decrease of the Si solubility in the metal in the lower mantle is due to the increase of Si coordination number in silicates from 4 (in the upper mantle and transition zone phases) to 6 (in silicate perovskite in the lower mantle). Alternatively, incorporation of silicon could occur by processes other than reaction 1. Ringwood and Hibberson (1991) studied the relative solubilities of several oxides in molten iron at 16 GPa and 1700–2000°C and concluded that mantle silicates could dissolve incongruently in molten iron, whereas simple oxides such as SiO_2 would dissolve congruently. Oxygen would then be associated with silicon as a light element in the core.

All the multianvil press investigations carried out to measure silicon incorporation in metal between 5 and 27 GPa (e.g., Ito and Katsura, 1991; Ito et al., 1995; Gessmann and Rubie, 1998;

* Author to whom correspondence should be addressed (Malavergne@lpi.usra.edu).

Gessmann et al., 1999, 2001; O'Neill et al., 1998) potentially suffer from problems with chemical equilibrium. These difficulties are intrinsic to the configuration of high-pressure and high-temperature experiments in multianvil press. For experimental durations long enough for equilibration to be reached, samples react with the assemblage because of the presence of molten metal in the studied systems. Moreover, temperature gradients are present in the samples (Rubie, 1999), especially at very high temperatures. Because it is impossible to avoid these problems with present technologies, studying reactions of exsolution of silicon out of metal, and comparing them with experiments measuring incorporation of silicon in metal, is a promising approach for better constraining equilibrium values.

The main purpose of the present study has thus been to perform experiments in which the starting metallic material is an Si-rich alloy, i.e., to study the process of reaction 1, but advancing from right to left, whereas most previous studies have been interested in its advancement from left to right. This study provided an opportunity to add new experimental data of solubility of silicon in metal at high pressures and temperatures to what is still a small global data set. These new experiments also made it possible measure precisely the correlation between the Fe contents in silicates, the Si contents in metal, the temperature, and the oxygen fugacity of the samples.

2. EXPERIMENTAL AND ANALYTICAL PROCEDURE

The metallic powders (FeSi and $Fe_{0.70}Si_{0.30}$) were obtained from GoodFellow (99.9% pure). The silicate powders used in these experiments were natural $(Mg_{0.88},Fe_{0.12})_2SiO_4$ olivine and $(Mg_{0.88},Fe_{0.12})SiO_3$ enstatite both from San Carlos (Arizona, USA), and a synthetic $MgSiO_3$ enstatite. Silicate powders were intimately mixed with one of the metallic powders listed above in a ratio of 80 or 85 wt% silicate, 20 or 15 wt% metal (Table 1).

Multianvil experiments were performed at the Bayerisches Geoinstitut, Bayreuth, Germany. Three samples (133, 134 and 135; Table 1) were synthesized at the French national multianvil facility in Clermont-Ferrand, France. The pressure assembly consisted of Cr-doped MgO octahedra with edge lengths of 14 or 10 mm. The octahedra were compressed using 32 mm carbide anvils with truncation edge lengths of 8 or 4 mm, with 14 and 10 mm octahedra respectively. The samples were contained in MgO capsules. Components of the high-pressure assemblies were initially fired at 1000°C for several hours before being assembled, except for the Mo disks, which allowed electrical contact between the heater and the power supply. The assembled octahedra were dried in a vacuum oven at 230°C overnight before each experiment. In all experiments the temperature was monitored with an axial $W_3Re/W_{25}Re$ thermocouple. Alumina ceramics insulators encased the wires of thermocouple and the thermocouple junction was placed in direct contact with the top of the MgO capsule. The samples were first pressurized at room temperature and then heated in the range 1600–2200°C for durations ranging from 80 s to 2 h (Table 1). As no correction was made for possible effect of pressure on the emf of the thermocouple, the maximum uncertainty is estimated to be ±100°C (Agee et al., 1995) for the highest temperature experiments. The samples were quenched by switching off the electrical power and the quench rate was

Table 1. Experimental conditions, starting materials (wt%), metallic phases compositions (in wt%), $\log(fO_2)$ relative to the IW buffer and phases observed after reaction at high pressure and high temperature.

Run	133	134	135	2851	2860	2559	2561	2416	2415	2414	2413
P (GPa)	10	10	10	10	20	20	20	25	25	25	25
T (°C)	2000	2000	2000	2000	2000	2200	2200	2000	1600	1600	2000
CEL/TEL (mm)[a]	14/8	14/8	14/8	14/8	10/4	10/4	10/4	10/4	10/4	10/4	10/4
Time	15 mn	15 mn	30 mn	10 mn	80 s	11 mn	7 mn	1 h	2 h	1 h	30 mn
Si in metal starting material[b]	17 (±0.2) (15wt%)	33 (±1) (15wt%)	17(±0.2) (15wt%)	17(±0.2) (15wt%)	17(±0.2) (15wt%)	33 (±1) (15wt%)	17(±0.2) (15wt%)	33 (±1) (15wt%)	33(±1) (15wt%)	17(±0.2) (15wt%)	33 (±1) (15wt%)
Silicate and N_{Fe} starting material	Ol 0.113 (±0.009)	Ol 0.113 (±0.009)	Ens 0.108 (±0.008)	Ens 0.108 (±0.008)	Ens 0.108 (±0.008)	Ol 0.113 (±0.009)	Ens 0.108 (±0.008)	Ens 0.108 (±0.008)	Ens 0.108 (±0.008)	Ens 0.108 (±0.008)	Ens 0.108 (±0.008)
Si in metal	16.5 (±0.18)	1.1 (±0.02)	0.7 (±0.01)	3.0 (±0.04)	7.6 (±0.07)	9.9 (±0.03)	17.6 (±0.12)	16.0 (±0.09)	32.0 (±0.15)	17.0 (±0.09)	28.0 (±0.13)
Phases observed	Met-ol	Met-ol-py	Met-ens-py	Met-ol	Met-sti-beta-maj	Met-sti-beta-pv	Met-sti-maj	Met-pv	Met-pv	Met-pv	Met-pv
ΔIW	−4.70	−3.30	−2.60	−3.70	−3.40	−3.80	−3.95	−4.00	−4.25	−4.10	−4.20

[a] CEL = tungsten carbide cube edge length; TEL = octahedra truncation edge length.

[b] Relative proportions of Si-rich alloy in the starting material are given between brackets. Analyses of the starting materials were all made with electron microprobe (see text for conditions). N_{Fe} is the Fe/(Fe + Mg) ratio in at%. Met = metal phase; ol = olivine; py = pyrope; ens = enstatite; sti = stishovite; beta = wadselyite; maj = majorite; pv = silicate perovskite. ΔIW : $\log(fO2)$ relative to IW buffer.

Table 2. Metallic phases and silicate compositions (in wt%) determined by EDX (SEM) in the 10 GPa samples. Oxygen is always below the detection limit of the used EDX systems.

Run	133	134		135		2851
Metal						
Fe	85.5 (±0.33)	98.9 (±0.31)		99.3 (±0.31)		97.0 (±0.28)
Si	16.5 (±0.18)	1.1 (±0.02)		0.7 (±0.01)		3.0 (±0.4)
n	12	10		8		10
Silicate	Olivine	Olivine	Pyrope	Enstatite	Pyrope	Olivine
Fe	0.45 (±0.01)	1.47 (±0.03)	0.74 (±0.02)	3.27 (±0.05)	1.65 (±0.02)	1.17 (±0.02)
Si	19.95 (±0.21)	19.81 (±0.21)	20.27 (±0.23)	27.49 (±0.30)	21.05 (±0.23)	20.04 (±0.21)
Mg	34.22 (±0.32)	33.13 (±0.31)	17.34 (±0.18)	22.15 (±0.24)	16.74 (±0.17)	33.54 (±0.31)
O[a]	45.38	45.60	48.31	46.77	47.39	45.25
Ca	—	—	0.89 (±0.16)	—	0.91 (±0.13)	—
Al	—	—	12.45 (±1.22)	0.32 (±0.08)	12.26 (±0.12)	—
n[b]	7	4	5	4	4	5
N_{Fe}[c]	0.006 (±0.002)	0.020 (±0.002)	0.017 (±0.002)	0.060 (±0.003)	0.040 (±0.003)	0.015 (±0.002)

[a] Oxygen is calculated by stoechiometry.
[b] *n* is the number of analysis.
[c] N_{Fe} is the Fe/(Fe + Mg) ratio in at%.

approximately 500°C/s. The samples were then decompressed overnight (12 h). After decompression, the charges were mounted in epoxy resin, sectioned, and polished to reveal the centers of the octahedra for analysis. Pressure calibrations of these experimental configurations are given in Tronnes and Frost (2002).

Samples were analyzed with a LEO STEREOSCAN 440 Scanning Electron Microscope (SEM) with PRINCETON GAMMA-TECH (PGT) SPIRIT energy-dispersive X-ray analyzer (EDX) able to analyze oxygen (20 kV; 2 nA). Counting times for analyses were of ~100 s for each EDX analysis and of 1 s per point for quantitative composition maps. Even though oxygen can be quantitatively analyzed with this SEM-EDX system, it was not possible to detect less than 1 wt% with our configuration. Standards used were pure Fe metal for Fe, wollastonite, quartz or FeSi for Si, MgO for Mg, Al_2O_3 for Al and CaO for Ca. A CAMECA SX electron probe microanalyzer (EPMA) equipped with wavelength dispersive X-ray spectrometer (WDX) and operating at 15 kV was also used to analyze the starting material and the four samples pressurized at 25 GPa. Two monochromators detected the first order reflection of K emission lines: LiF (200) for the K_α peak of Fe, TAP (1011) for Si K_α and Mg K_α. The counting times with EPMA were 10 s (for Si and Mg) and 20 s (for Fe), and a typical beam current of 10 nA was used. The standards used were Fe_2O_3 for Fe, enstatite for Si and Mg.

Three samples (runs 2559, 2561 and 2413) were examined with a JEOL 2000 EX Transmission Electron Microscope (TEM) equipped with a Tracor TN 5400 FX X-ray analyzer. Polished thin slides were made out of each sample, then mounted on 3 mm Cu rings with a central single hole of diameter 600 μm and thinned by an argon-ion beam with a voltage of 3.5 kV and currents of 0.5 mA at each cathode, until perforation of the samples. Samples were finally coated with a thin film of carbon to prevent sample charging effects. Microanalyses were carried out in scanning transmission mode. EDX microanalyses using TEM were recorded with collecting times ranging between 30 and 150 s with 8000 to 15,000 net counts for the major elements. Elemental ratios were measured in the standards (olivines and enstatites from San Carlos, Arizona, USA) for different thicknesses and were then extrapolated to zero-thickness to extract the experimental K-factors (a theoretical parameter proportional to the ratio of concentration of the analyzed element) (Van Cappelen, 1990). The possibility of measuring properly Fe/Fe + Mg ratios as low as 1% in silicates from silicate-metal assemblages such as those studied here, without suffering from X-ray pollution from adjacent metal particles, was tested on unreacted assemblages. Even if the analytical precisions decrease from EPMA to EDX-SEM to EDX-TEM, all methods are mutually consistent, as seen in Tables 2 to 7.

3. RESULTS

Under the pressure-temperature conditions of the experiments (Table 1), the metal was always liquid, as shown by

Table 3. Metallic phases compositions (in wt%) determined by EDX (SEM and ATEM) in the 20 GPa samples. Oxygen is always below the EDX detection limits.[a]

	2561			2860			2559	
Run	SEM	ATEM	EEM[a]	SEM	EEM[a]	SEM	ATEM	EEM[a]
Fe	82.2 (±0.33)	83.4 (±1.2)	84.2 (±5.6)	92.4 (±0.63)	93.4 (±5.3)	90.1 (±0.33)	89.3 (±0.83)	82.3 (±3.3)
Si	17.8 (±0.12)	16.6 (±0.67)	15.8 (±4.5)	7.6 (±0.12)	6.6 (±2.3)	9.8 (±0.03)	10.7 (±1.6)	8.3 (±3.1)
n	60	11	—	50	—	50	13	—

[a] EEM = end-member extrapolation method (see text and Fig. 2).

Table 4. Metallic phases compositions (in wt%) determined by EDX (SEM and ATEM) and EPMA in the 25-GPa samples,

	2416		2415		2414		2413		
Run	*SEM*	*EPMA*	*SEM*	*EPMA*	*SEM*	*EPMA*	*SEM*	*EPMA*	*ATEM*
Fe	83.9 (±0.32)	83.51 (±0.21)	67.8 (±0.31)	667.48 (±0.23)	83.1 (±0.32)	82.26 (±0.26)	73.1 (±0.29)	71.15 (±0.21)	72.4 (±1.7)
Si	16.1 (±0.15)	15.91 (±0.09)	32.2 (±0.17)	31.87 (±0.10)	16.9 (±0.11)	17.13 (±0.08)	27.9 (±0.11)	28.10 (±0.09)	27.5 (±1.5)
Total	—	99.42	—	99.35	—	99.39	—	99.25	—
n	40	25	20	10	22	10	60	21	15

textural evidences (see below), except in the two samples heated at 1600°C at 25 GPa where no evidence for melting were found. These observations are in good agreement with melting determinations in pure Fe at high pressure by Boehler (1993), Andrault et al. (1997), and Lin et al. (2002). Moreover, Yang and Secco (1999) found a melting temperature of 1430°C at 5.5 GPa for Fe-17 wt% Si. Therefore, the observed liquid state of alloys in all 10 and 20 GPa experiments is consistent and reinforced by the fact that silicon decreases the melting point of iron. Compositions of the metal and silicate phases in the experimental products are given in Tables 1 through 6.

Two classes of samples can be distinguished. On one hand, samples at 20 and 25 GPa and one sample at 10 GPa (run 133) only showed minor exchange with the container and external materials from the cell assembly. W has never been detected neither in capsules nor in samples. No reaction between the sample and the thermocouples were observed in all the samples of the present study. On the other hand, three out of the four 10 GPa samples reacted rather strongly with the container and other external materials, the reaction being more prominent as experimental time increased, as shown by the increasing oxidation rate of samples with time in the 10 GPa samples. For example, two samples, 135 and 2851, were both made from the same starting material. Their run durations and oxygen fugacities relative to IW are 30 mn, 10 mn and −2.60, −3.70, respectively (Table 1). Although these samples obviously suffered from global disequilibrium, they still have some interest because local equilibrium has likely been reached at metal/silicate interfaces, as evidenced by the absence of chemical zoning (Fig. 1). A reason why samples at 10 GPa reacted more with the cell assembly than other samples might be the positive pressure effect on melting curves for various materials in the cell assembly and in the starting materials.

In all samples, oxygen was not detected in metal phase. Using data of O'Neill et al. (1998), it is possible to infer the oxygen content that should be present in the metal in the present study. At all conditions investigated, calculated values are of less than 1 wt% of oxygen in metal, below the detection limit for oxygen with the analytical systems used in the present study.

3.1. 10 GPa Samples

In these samples, the metal phases were strongly depleted in silicon relative to the starting metal compositions except for run 133. The silicon contents of metal phases after reaction are given in Tables 1 and 2, and the composition of silicates are given in Table 2 as well as the Fe/(Fe + Mg) ratios in coexisting silicates. In these samples, the Fe content N_{Fe} (N_{Fe} = Fe/(Fe + Mg)) of the silicates decreases strongly by 40 to 95% showing that the silicate starting material has been strongly reduced. The metal phase is most often of quasi-spherical shape within the silicate matrix, which mostly consists of olivine. Samples 133 and 2851 have experienced some reaction only with the MgO capsule. In samples 134 and 135, reaction with alumina from thermocouple ceramics resulted in the presence of an aluminous phase, pyrope, coexisting with enstatite or olivine. Differences in starting materials, various amounts of reactions, and exchange rates of oxygen species between sample and assemblage, explain the differences between the final compositions of the four samples recovered from 10 GPa (Tables 1 and 2).

3.2. 20 GPa Samples

At 20 GPa, reactions of the samples with the cell assemblies were much less pronounced than at 10 GPa. Very similar

Table 5. Silicate phases compositions (in wt%) determined by EDX analysis (SEM and ATEM) at 20 GPa and 2000°C–2200°C.

	2860 wadsleyite	2860 majorite	2559 wadsleyite	2559 perovskite	2559 wadsleyite	2559 perovskite	2561 majorite	2561 majorite
Run	SEM	SEM	SEM	SEM	ATEM	ATEM	SEM	ATEM
Fe	3.38 (±0.055)	1.69 (±0.033)	0.78 (±0.015)	0.56 (±0.010)	0.60 (±0.11)	0.57 (±0.10)	0.54 (±0.010)	0.64 (±0.12)
Si	19.59 (±0.21)	27.74 (±0.28)	19.92 (±0.20)	27.92 (±0.27)	20.70 (±0.35)	25.98 (±0.51)	27.90 (±0.27)	28.92 (±0.58)
Mg	32.53 (±0.32)	23.18 (±0.22)	33.78 (±0.31)	23.70 (±0.22)	33.10 (±0.72)	23.05 (±0.65)	23.73 (±0.22)	22.11 (±0.63)
O[a]	44.50	47.39	45.52	47.82	45.6	50.4	47.83	48.33
n	15	8	30	13	10	8	20	22
N_{Fe}[b]	0.030 (±0.002)	0.030 (±0.002)	0.010 (±0.003)	0.010 (±0.003)	0.009 (±0.002)	0.010 (±0.002)	0.010 (±0.003)	0.011 (±0.002)

[a] Oxygen is calculated by stoechiometry.
[b] N_{Fe} is the Fe/(Fe + Mg) ratio in at%.

Table 6. Silicate phases compositions (in wt%) determined by EDX analysis (SEM, ATEM) and by electron microprobe (EPMA) at 25 GPa.

	2416 perovskite		2415 perovskite		2414 perovskite		2413 perovskite		
Run	SEM	EPMA	SEM	EPMA	EPMA	SEM	ATEM	SEM	EPMA
Fe (FeO)[a]	0.33 (±0.03)	0.369 (±0.005)	0.45 (±0.02)	0.58 (±0.01)	0.54 (±0.01)	0.39 (±0.015)	0.54 (±0.08)	0.52 (±0.015)	0.80 (±0.02)
Si (SiO2)[a]	27.95 (±0.26)	60.05 (±0.35)	27.93 (±0.25)	59.98 (±0.34)	60.11 (±0.34)	27.93 (±0.26)	28.01 (±1.01)	28.17 (±0.27)	60.02 (±0.34)
Mg (MgO)[a]	23.80 (±0.22)	39.36 (±0.10)	23.75 (±0.21)	39.95 (±0.11)	39.13 (±0.11)	23.78 (±0.22)	23.79 (±0.92)	23.56 (±0.21)	39.06 (±0.10)
O	47.92		47.87			47.90	47.66	47.75	
(Total)[a]		99.78		100.51	99.78				99.88
n	23	10	13	8	6	18	10	10	16
N_{Fe}[b]	0.006 (±0.0015)	0.006 (±0.001)	0.008 (±0.0015)	0.008 (±0.001)	0.007 (±0.001)	0.007 (±0.0015)	0.010 (±0.002)	0.010 (±0.002)	0.011 (±0.002)

[a] For EPMA analysis only.
[b] N_{Fe} is the Fe/(Fe + Mg) ratio in at%.

Table 7. Slopes of regression lines from Figure 7. Temperatures of experiments are between 2273 K and 2473 K.

Pressure	Slope	Regression coefficient
5 GPa[a]	−0.72 (±0.23)	0.771
9–10 GPa[b]	−0.57 (±0.15)	0.833
10 GPa[c]	−0.71 (±0.08)	0.918
18 GPa[d]	−0.824 (±0.04)	0.948
20 GPa[e]	−0.79 (±0.01)	0.955
23–25 GPa[de]	−0.74 (±0.02)	0.978

[a] Gessmann et al. (2001) and Li and Agee (2001b).
[b] O'Neill et al. (1998), Gessmann et al. (2001), and Li and Agee (2001).
[c] Our study.
[d] O'Neill et al. (1998) and Gessmann et al. (2001).
[e] O'Neill et al. (1998), Gessmann et al. (2001), Ohtani et al. (1997), and Li and Agee (2001).

observations have been made in samples 2559, 2561 and 2860. First, an oxidation of Si_{metal} into SiO_2 is observed as reaction rims around metal particles (Figs. 2 and 3). ATEM observations demonstrate that the SiO_2 phase in reaction rims around the metal phase is stishovite (Fig. 3). These rims of stishovite are particularly visible around the largest metal particles (typical size between 15 and 60 μm) as shown in Figure 2, but smaller grains of stishovite are also present in close association with smaller metallic particles (typical size between 1 and 5 μm). Farther away of the largest metal particles, the silicate matrix is made of majorite and/or wadsleyite, depending on the

Fig. 1. (a) Composition profile in sample 2851 (10 GPa, 2000°C): SEM image (backscatttered electrons) and composition profile plotted as Si/Fe ratio vs. beam position (μm). (b) Zoom of the chemical profile in the metal phase plotted in Si/Fe vs. beam position (μm) diagram.

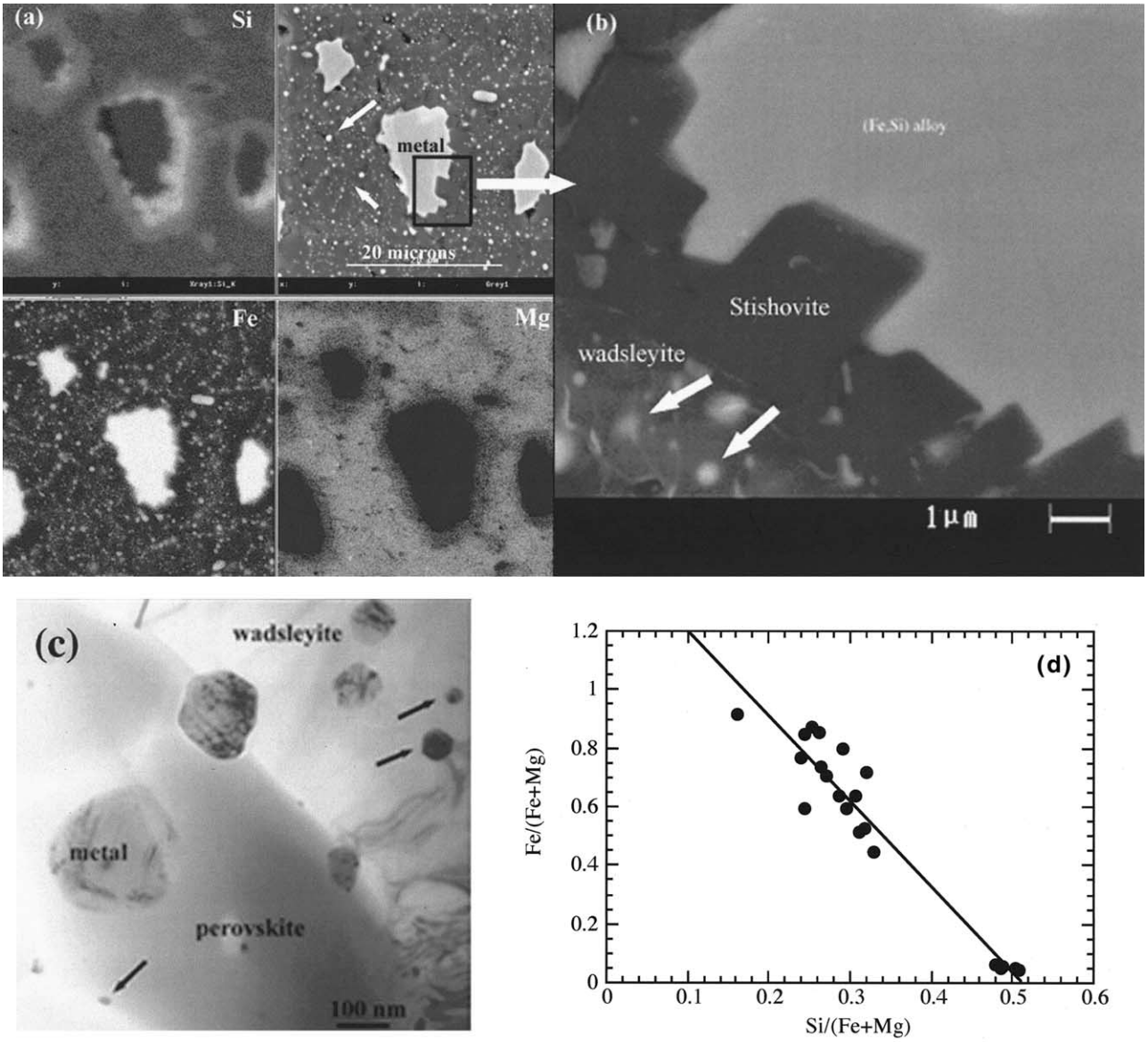

Fig. 2. (a) Composition maps obtained with the EDX system of the SEM on sample 2559 (20 GPa–2200°C) showing the SiO_2 reaction rim around metal grains. The SEM electron micrograph (backscattered electrons) shows the two populations of metal particles: large grains inherited from the initial grains, and tiny quasi-spherical particles due to reduction of the iron-bearing silicate starting materials. Both populations have the same composition. (b) Detail of the metal silicate interface as seen by backscattered electrons in SEM. The coexistence of stishovite and wadsleyite is consistent with the equilibrium phase diagram in the Mg-Fe-Si-O system at these pressure and temperature. Tiny metal particles (arrows) are clearly visible within wadsleyite. Their compositions, analyzed by ATEM are identical to that of large metal areas showing that local equilibrium conditions are achieved in the samples. (c) TEM electron micrograph of sample 2559 showing small metallic particles (arrows) as well as larger metal particles in the silicate matrix (wadsleyite and silicate perovskite). (d) EDX analyses of tiny metallic particles in sample 2559 plotted in an Fe/(Fe + Mg) vs. Si/(Fe + Mg) diagram. The beam size was larger than the mean size of metal particles and metal-free wadsleyite areas. End-member compositions can be retrieved at (Fe/(Fe + Mg) = 1 (metal phase) and Si/(Fe + Mg) = 0.5 (wadsleyite). The intersection between the regression line and the line Fe/(Fe + Mg) is 0.165 providing 8.3 wt% of Si in metal in the smallest particles of alloy. The slope of the regression line is –2.89 with correlation coefficient R = 0.986.

starting silicate used in the experiment. The presence of SiO_2, wadsleyite or majorite is in good agreement with the phase diagram of $MgSiO_3$ at 20 GPa and high temperature (2000–2200°C) (Gasparik, 1990). Wadsleyite and majorite contain quasi-spherical metal phases as seen in Figure 2. The size of the small metal particles ranges between 15 nm and 500 nm (Fig. 2). These observations show that a reduction of the silicates has taken place. This is also shown by the depletion of their Fe content. For example in the run 2860 (20 GPa and 2000°C), the Fe content N_{Fe} (N_{Fe} = Fe/(Fe + Mg)) of the silicate decreases from 0.108 to 0.03, showing a depletion of ~75% of its iron (Tables 1 and 2). In the samples 2559 (20 GPa and 2200°C) and

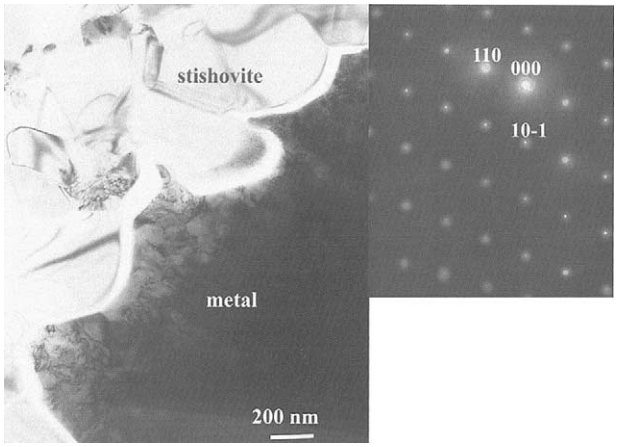

Fig. 3. TEM electron micrograph of the metal-silicate interface in sample 2559. The growth of the stishovite phase at the expense of the metal phase is particularly visible from the shape of the interface. Stishovite may come both from silicates, exsolved as a result of FeO loss to maintain stoichiometry, and from FeSi alloy, oxidation of Si. Insets are diffraction patterns of the stishovite phase, with cell parameters of a = 4.17 ± angstrom and c = 2.66 ± angstrom and space group P4/mnm (tetragonal system).

2561 (20 GPa and 2200°C), the silicates have lost ~90% of their iron.

To study the tiny microstructures evidenced by SEM (Fig. 2), samples 2559 and 2561 were examined with the TEM. The iron-silicon alloys have either tetragonal (space group P4/mmm) or cubic (space group Pm3m) structures. Because of reaction, these alloys have been depleted in silicon even in the largest particles. The electron beam size of SEM or TEM was larger than the mean size of the tiny particles, as it is shown in Figure 2. Even with TEM, it was impossible to analyze quantitatively the smallest metal particles without contamination from the silicate matrix. The knowledge of Si content in metal is however essential to constrain local equilibrium in the samples. Therefore, we used extrapolations to end-members (EE) to estimate the chemical compositions of the smallest particles of metal by plotting chemical analyses of Fe/(Fe + Mg) vs. Si/(Fe + Mg) (Fig. 2). As the metal does not contain magnesium, it is possible to extrapolate the metal composition of the small particles to a ratio of Fe/(Fe + Mg) = 1. With this method, the iron content of silicate could be estimated for ratios of Si/(Fe + Mg) = 0.5 in wadsleyite and Si/(Fe + Mg) = 1 in silicate perovskite and majorite. This EE method allowed us to estimate the composition of the small metal grains and to compare it to that of the larger particles. It is less precise than direct EDX analysis because of the scatter of the data in the diagram (Fig. 2) and because analyses of tiny metal particles are always contaminated by some silicate matrix. Nevertheless, we find a good correlation between the different EDX analyses and EE results as shown in Table 4. We find that the large particles of metal in contact with silicates have the same silicon content (Table 3) as the tiny metal grains embedded within the silicate matrix. This is a first indication for local equilibrium at the scale of several tens of micrometers in these samples; a second indication is the absence of chemical zoning as shown in Figure 4. The differences in compositions of phases in those different samples is because of different starting material compositions. In these 20 GPa samples, starting either from olivine or from enstatite yields samples all having SiO_2 stishovite expressed in contact in metal. This emphasizes that the phase controlling incorporation in metal is the same (i.e., SiO_2) whether the starting material was olivine or enstatite. Some incorporation of silicon could also have occurred by congruent dissolution of SiO_2 in metal (Ringwood and Hibberson, 1991). Small amounts of stishovite might thus have been extracted into the molten metal. On the basis of the results of Ringwood and Hibberson (1991), this contribution would remain small because they observed an SiO_2 solubility of ~0.9 wt% in iron at 16 GPa and ~1900°C. The fact that this contribution is small is confirmed by the nondetection of oxygen in the alloys.

3.3. 25 GPa Samples

In the four samples synthesized at 25 GPa using iron-free enstatites as silicate starting materials, no stishovite was found. Only Mg-silicate perovskite and metal alloys were observed. After reaction, those samples were characterized by a slight increase in Fe-content in the silicate phase (up to 1 at% Fe in silicate pervoskite, Table 6), and basically no detectable changes in Si content of the metal (Tables 1 and 4). At 2000°C, the FeSi alloys have a CsCl cubic structure (space group Pm-3m) as found recently by Dobson et al. (2002). No reaction occurred between the assembly and the samples. The runs at 25 GPa lasted between 30 mn and 2 h, long enough to reach equilibrium (e.g., Othani et al., 1997; Gessmann and Rubie, 1998) in the center of the samples.

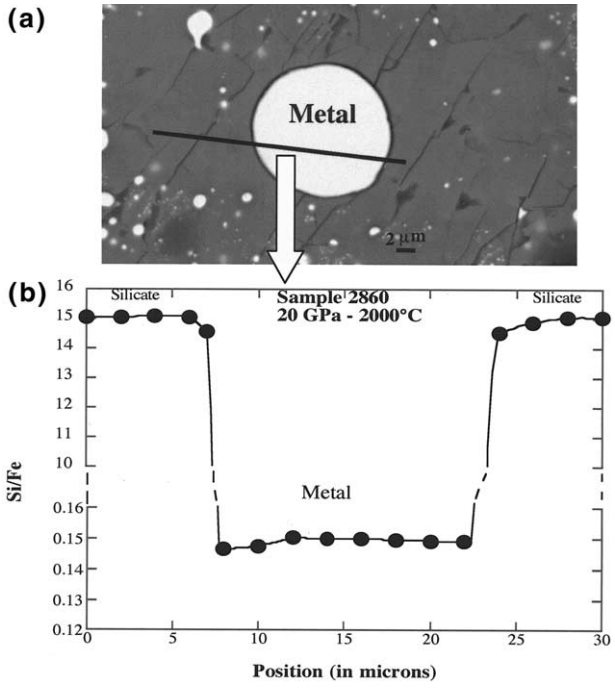

Fig. 4. (a) Chemical profile of sample 2860 (20 GPa, 2000°C): SEM image showing the line where the analysis were made and composition profile plotted in Si/Fe vs. beam position (in μm) diagram. (b) Zoom of the chemical profile in the metal phase plotted in Si/Fe vs. beam position (in μm) diagram.

4. DISCUSSION

This study allowed characterizations, down to the scale of transmission electron microscopy, of high-pressure and high-temperature reactions between mantle minerals and Si-rich metal alloys. Thanks to differences in oxygen contents of starting materials, and to various amounts of oxygen exchange with the rest of the assemblage, various oxygen fugacity conditions were investigated (Table 1). We believe that local equilibrium compositions have been attained in those experiments because we observe homogeneous element concentrations in both silicate and metal phases (Figs. 1 and 4). Also, Othani et al. (1997) and Gessmann and Rubie (1998) have demonstrated attainment of equilibrium in similar experiments in less than 4 min.

The redox conditions in each sample were first calculated relative to the iron-wüstite (IW) buffer from the iron contents in silicate and in metal in the run products at the relevant P,T conditions (Table 1). Oxygen fugacity relative to IW is defined by: $\log fO_2 = 2 \log(a_{FeO}/a_{Fe})$, where a_{FeO} and a_{Fe} are the activities of FeO in silicate and Fe in liquid metal, respectively. For Fe in iron rich alloys, the Raoult's law assumption generally applies (e.g., Hultgren et al., 1973); we thus assumed that the activity of Fe in the metal is equal to its mole fraction when $x_{Fe} > 0.70$. We calculated activity coefficients for FeO in different silicates using different sets of expressions (Fei and Saxena, 1986; Fei et al., 1991). The oxygen fugacities listed in Table 1 were calculated assuming that activity-composition relations in metal are independent of pressure. Application of different low P, T activity-composition relations in silicates and Fe alloy (Lacaze and Sundman, 1991; Bouchard and Bale, 1995; Schlesinger and Xiang, 2001) would lead to differences smaller than 0.6 log unit in estimated $\log fO_2$. We also estimated fO_2 from the SiO_2-Si buffer to test the calculations of fO_2 relative to IW. Oxygen fugacity relative to SiO_2-Si buffer is defined by: $\log fO_2 = \log(a_{SiO2}/a_{Si})$, where a_{SiO2} and a_{Si} are the activity of SiO_2 and the activity of Si in liquid metal, respectively. As SiO_2 is present in the 20 GPa samples, then $a_{SiO2} = 1$ in these samples. For metallic solutions with less than a few wt% Si, Henry's law applies well at 1 bar (Lacaze and Sundman, 1991; Bouchard and Bale, 1995; Schlesinger and Xiang, 2001). No data exist, however, to confirm this behavior at high pressure. For metals more concentrated in silicon, an intermediate regime between Henry's law and Raoult's law fitted to a polynomial applies (Matas et al., 2000). We assumed that the activity of Si in the metal in our study is equal to $a_{Si} = \gamma^0 x_{Si}$, where x_{Si} is the mole fraction of Si in the metal and γ^0 the Henry coefficient. It is thus possible to calculate the fO_2 of the experiment relative to IW buffer following the relation

$$\ln (fO_2)_{experiment} = \ln fO_2(\text{IW at 1 bar}) + 2\int \Delta V \, dP/(RT) + 2 \ln (a_{FeO\ silicate}/a_{Fe\ metal})$$

We can also calculate the fO_2 of the experiment relative to SiO_2-Si buffer following the relation:

$$\ln (fO_2)_{experiment} = \ln fO_2(SiO_2 - Si \text{ at 1 bar}) + \int \Delta V \, dP/(RT) + \ln (a_{SiO_2}/a_{Si\ metal})$$

The ΔV for each equation is calculated from the data of Poirier (1991) and Robie et al. (1979) for Si and Fe liquid and Fei and Saxena (1986) using a second-order Birch-Murnaghan equation for FeO and stishovite. As an example, Figure 5a shows the oxygen fugacity calculated as a function of temperature from the IW buffer and from the SiO_2-Si buffer for one 20 GPa experiment. The intersections of the two lines in Figure 5 should give the temperature of the experiment if these data are consistent. We find temperatures ranging between 2200°C and around 2000°C for the three 20 GPa runs, which is indeed in very good agreement with the measured experimental temperatures. The correlation between Si in metal and Fe in silicates as a function of fO_2 is thus well constrained from two consistent methods.

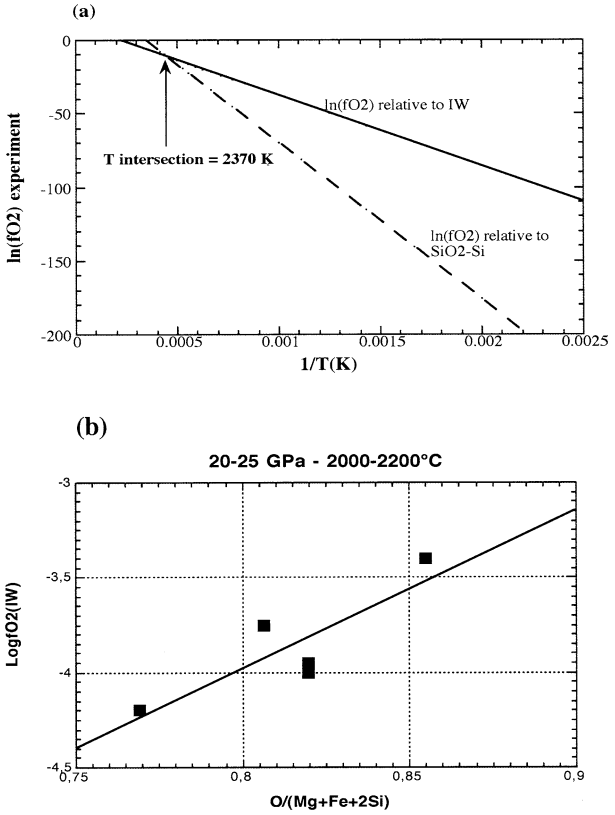

Fig. 5. (a) Oxygen fugacity calculated as a function of temperature from the IW buffer and from the SiO_2-Si buffer for experiment 2559 (20 GPa –2200°C). (b) Oxygen fugacity relative to IW as a function of O/(Mg + Fe + 2Si) ratio of the starting material. This correlation is shown at 20–25 GPa and 2000–2200°C. The fO_2 has been calculated on the basis of the Fe-FeO compositions determined in the quenched samples.

The effect of using different starting materials to vary the redox conditions is shown in Figure 5b, in which calculated oxygen fugacities are plotted as a function of the O/(Fe + Mg + 2Si) ratio of the starting material. Other proxies for characterizing the oxygen content of the starting materials could have been used. The Si content in metal is related to oxygen fugacity by:

$$Si_{metal} + O_2 \leftrightarrow SiO_{2\ silicate} \quad (2)$$

The mole fraction $X_{Si_{metal}}$ of Si in metal may be described by the equations:

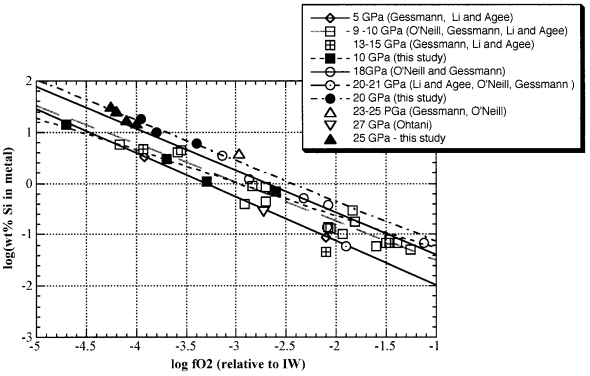

Fig. 6. Summary of experimental results of this study and previous work by Gessmann et al. (2001), Li and Agee (2001b), O'Neill et al. (1998), Kilburn and Wood (1997), Othani et al. (1997) and Ito et al. (1995). The experimental Si contents in metal are plotted vs. fO_2 relative to IW at different pressures. Temperatures of all experiments are between 2000°C and 2200°C. Similar symbols (triangle, square, circle) represent a given P.

$$\log (X_{Si_{metal}}) = A(T,P) - \log\ (a_{Si})_{metal} - \log (a_{SiO_2})_{silicate} - 2 \log (a_{FeO\ silicate}/a_{Fe\ metal}) \quad (4)$$

$$\log (X_{Si_{metal}}) = A(T,P) - \log (a_{Si})_{metal} - \log (a_{SiO_2})_{silicate} - \log fO_2(\text{relative to IW}) \quad (5)$$

where $A(T,P) = -\Delta_r G(T,P)/RT$ is a parameter depending only on pressure and temperature. From reaction 2 and Eqn. 5, the theoretical slope of a diagram that represents $\log(X_{Simetal})$ vs. $\log fO_2$ (relative to IW) can be deduced (e.g., Gessmann et al., 1999, 2001). It should be -1 if the valence of Si is 4+ and if Henry's law or Raoult's law applies. Our data set and previous results give slopes of regression lines of logwt%Si-$\log fO_2$ diagrams at a given P and T ranging between -0.57 and -0.83 instead of -1 for ideal models (Table 7). This discrepancy is probably the result of nonideal mixing properties of Si. If the activity of Si in metal was better known, it could be possible to evaluate the mean actual valence of Si. Indeed, in Table 1, we notice that some data points corresponding to almost the same fO_2, are associated to very different concentrations of Si in metal (e.g., experiments 2415 and 2413). The precision of the estimated of fO_2 does not allow to actually differentiate those data for oxygen fugacities. The different silicon contents in metal from these experiments result from the strong dependence of the solubility of Si in metal upon fO_2, implying that small differences in fO_2, even undetectable by our measurements, can change Si content in metal.

The measured silicon content in metal are summarized in Figure 6 as a function of oxygen fugacity calculated from Fe contents in metal and coexistent silicates, at different pressures, both from this study and from published data. Our experiments performed with Si-rich alloys as starting materials are consistent with previous data, using generally Si-poor metal phases as starting materials. Such a good overall concordance suggesting that the data obtained from multianvil press studies reflect equilibrium values. Although global disequilibrium may still exist in multianvil press experiments as a result of incomplete reaction and ongoing oxygen transfer between sample and assemblage, these results indicate an approach of equilibrium with Si contents in metal that is consistent with models derived from experimental high-pressure data, such as that of Gessmann et al. (2001). Because some of the experimental results plotted in Figure 6 involved equilibrium of liquid metal with molten silicates, whereas in others only solid silicates were involved, the concentration of Si_{metal} in equilibrium with silicates does not depend critically on the solid or liquid state of the silicate as well as on the exact nature of the silicate, provided that the P, T, fO_2 conditions are similar.

Chabot and Agee (2003) found that the depletion of slightly siderophile elements in the mantle can be explained by core-mantle equilibration at high temperature and an fO_2 of about ΔIW-2.3 log unit. It is of interest to estimate on the amount of Si that would enter into liquid metal at such fO_2, around 20–25 GPa and 2000°C. The 20 and 25 GPa data were corrected to 2.3 $\log fO_2$ units below IW thus decreasing the Si mol fraction in the metal by 0.8 log unit for every 1 log unit increase in fO_2, on the basis of the dependence of Si solubility on fO_2 (Fig. 6). After correction of our experimental data to the oxygen fugacity of ΔIW-2.3 log units, the x_{Si} in metal is < 0.01 at 10 and 20 GPa, and < 0.007 at 25 GPa, in good agreement with the model of Gessmann et al. (2001). Earlier studies of Ni and Co partitioning (e.g., Thibault and Walter, 1995; Righter et al., 1997; Li and Agee, 1996, 2001a) suggested that the mantle siderophile elements content requires core formation at fO_2 near IW-1 log unit. These last results imply that almost no Si could enter to the metal during the segregation of the core under such conditions. In this case, mechanisms involving sequestration of Si in the lower mantle as a result of perovskite fractionation in an early magma ocean should be invoked for explaining the "missing" Si (Anderson, 1988; Javoy, 1995).

As already noticed by Gessmann et al. (2001), it is possible to make an Earth core with 7 wt% Si and an Earth mantle with silicates having Fe/Fe + Mg = 0.1 if metal/silicate segregation occurred at 20 GPa, 2400°C (Fig. 7). Increasing pressure would

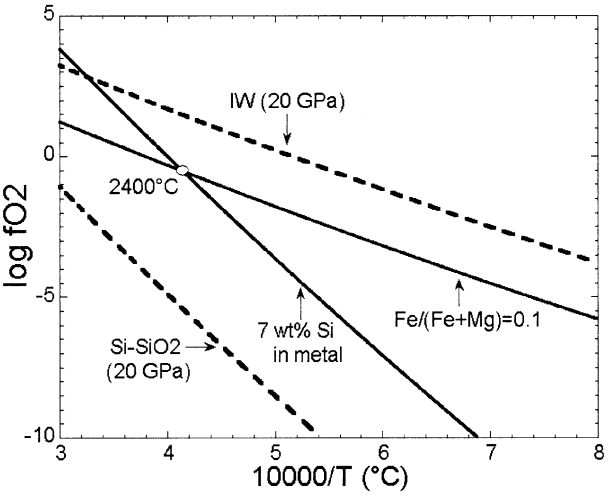

Fig. 7. Oxygen fugacity calculated at 20 GPa as a function of temperature from the IW buffer, from the SiO_2-Si buffer, from an alloy equilibrated with 7 wt% of Si in metal, from a metal in equilibrium with a silicate that has a Fe/(Fe + Mg) ratio of 0.10 (average ratio for the silicates of the mantle).

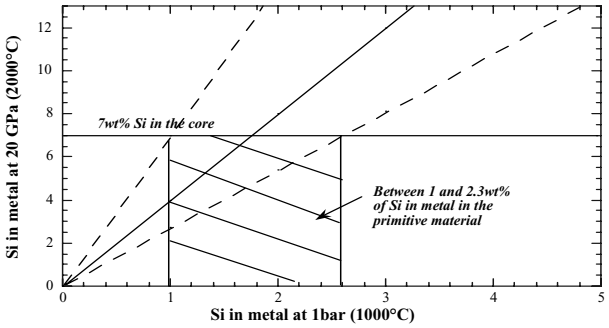

Fig. 8. Silicon content in metal at 20 GPa and 2000°C as a function of the Si in metal equilibrated with silicates at lower pressure and temperature (1 bar and 1000°C) after reaction 1. The 20 GPa–2000°C conditions might correspond to the conditions of a final Earth-like material and 1 bar–1000°C is indicative of a small planetary body. We use the present 20 GPa experimental data (x_{Fe} in metal, x_{Si} in metal and x_{Fe} in silicate) and thermodynamical data of Robie et al. (1979) and Bouchard and Bale (1995) for these calculations. The two dashed lines indicate the maximum and minimum uncertainties from these calculations. The horizontal line indicates 7 wt% Si required in the core according Javoy (1995) or Allègre et al. (2001).

not favor incorporation of more silicon in the metal (Javoy, 1995; Guyot et al., 1997; Gessmann et al., 2001; Hillgren and Boehler, 1998; Dubrovinsky et al., 2003). The Earth is formed through accretion of many small bodies called planetisimals with an initial kilometer-sized radius (e.g., Hayashi et al., 1985; Wetherill, 1994; Kokubo and Ida, 2000). The internal pressure of these planetisimals depends obviously on their size, temperature and density, but stays very low in comparison with the Earth's upper mantle pressure. We have made the assumption that a small planetisimal could be equilibrated at 1 bar (low pressure) and 1000°C (high temperature), which is in agreement with the results of Yoshino et al. (2003). The Si content of an Fe-Si alloy equilibrated with FeO and SiO_2 after reaction 1 at 20 GPa and 2000°C is plotted in Figure 8 vs. the Si content resulting from the same equilibration at low-pressure parent body–like conditions (1 bar−1000°C) (e.g., Wetherill, 1994; Yoshino et al., 2003). This plot emphasizes the well known statement that reduced conditions (below IW) are needed for significant silicon incorporation in metal (e.g., Gessmann et al., 2001) even when high pressure and high temperatures characteristic of the differentiating Earth are involved. Moreover, Figure 8 offers a qualitative relationship between the silicon content in the metal of a final Earth-like material reacted at 20 GPa and 2000°C and that in a small planetary body equilibrated at lower pressure and temperature. To reach ~7 wt% Si in the Earth's core as required by some geochemical models (e.g., Javoy, 1995; Allègre et al., 2001), an average value of ~1.5 wt% Si would be needed in the metal of a material equilibrated at low pressures and 1000°C.

Acknowledgments—High-pressure, high-temperature experiments were performed using a 1200-tonne multianvil apparatus at Bayerisches Geoinstitut (Germany), under the EU "IHP-Access to Research Infrastructures" Programme (contract 42 in 2000 and 2001 to D. C. Rubie) and using a 1200-tonne multianvil apparatus at the "Laboratoire Volcan et Magma," Clermont-Ferrand (France), under the French national facility of INSU. The article benefited considerably from detailed and constructive review by J. Li, C. Agee, one anonymous reviewer, and the comments of B. Mysen, who greatly improved the initial version.

Associate editor: F. Podosek

REFERENCES

Anderson D. L. (1988) Composition of the Earth. *Science* 243, 367–370.

Andrault D, Fiquet G., Kunz M., Visocekas F., and Häusermann D. (1997) The orthorhombic structure of iron: An in situ study at high-temperature and high-pressure. *Science* 278, 831–834.

Agee C. B., Li J., Shannon M. C., and Circone S. (1995) P-T phase diagram for the Allende meteorite. *J. Geophys. Res.* 100, 17725–17740.

Allègre C., Poirier J. P., Humler E., and Hofman A. (1995) The chemical composition of the Earth. *Earth Planet. Sci. Lett.* 134, 515–526.

Allègre C., Manhès G., and Lewin E. (2001) Chemical composition of the Earth and the volatility control on planetary genetics. *Earth Planet. Sci. Lett.* 185, 49–69.

Boehler R. (1993) Temperature in the Earth's core from melting-point measurements of iron at high static pressures. *Nature* 363, 534–536.

Bouchard D. and Bale C. W. (1995) Ti-Si Interaction in liquid iron. *Can. Metal. Q.* 34, 343–346.

Dobson D. P., Vocadlo L., and Wood I. G. (2002) A new high-pressure phase of FeSi. *Am. Mineral.* 87, 784–787.

Dubrovinsky L., Dubrovinskaia N., Langenhorst F., Dobson D., Rubie D., Gessmann C., Abrikosov I. A., Johansson B., Baykov V., Vitos L., Le Bihan T., Crichton W. A., Dmitriev V., and Weber H. P. (2003) Iron-silica interaction at extreme conditions and the electrically conducting layer at the base of the Earth's mantle. *Nature* **422,** 58–61.

Fei Y., Mao H-K., and Mysen B. (1991) Experimental determination of element partitioning and calculation of phase relation in the MgO-FeO-SiO_2 system at high pressure and high temperature. *J. Geophys. Res.* 96, 2157–2169.

Fei Y. and Saxena S. (1986) A thermochemical data base for phase equilibra in the system Fe-Mg-Si-O at high pressure and temperature. *Phys. Chem. Minerals* **13,** 311.

Gasparik T. (1990) Phase relations in the transition zone. *J. Geophys. Res.* 95, 15751–15769.

Gessmann C. K. and Rubie D. C. (1998) The effect of temperature on the partitioning of nickel, cobalt, manganese, chromium, and vanadium at 9 GPa and constraints on formation of the Earth's core. *Geochim. Cosmoschim. Acta* **62,** 867.

Gessmann C. K., Rubie D. C., and McCammon C. A. (1999) Oxygen fugacity dependence of Ni, Co, Mn, Cr, V and Si partitioning between liquid metal and magnesiowustite at 9–18 GPa and 2200°C. *Geochim. Cosmoschim. Acta* 63, 1853–1863.

Gessmann C. K, Wood B. J, Rubie D. C., and Kilburn M. R. (2001) Solubility of silicon in liquid metal at high pressure: Implications for the composition of the Earth's core. *Earth Planet. Sci. Lett.* 184, 367–376.

Goarant F., Guyot F., Peyronneau J., and Poirier J. P. (1992) High pressure and high temperature reactions between silicates and liquid iron alloys, in the diamond anvil cell, studied by analytical electron microscopy. *J. Geophys. Res.* 97, 4477–4487.

Guyot F., Zhang J., Martinez I., Matas J., Ricard Y., and Javoy M. (1997) P-V-T measuremants of iron silicide (ε-FeSi). Implications for silicate-metal interactions in the early Earth. *Eur. J. Mineral.* 9, 277–285.

Hayashi C., Nakazawa K. and Nakagawa Y. (1985) Formation of the solar system. In *Protostars and Planets II* (eds. D. C. Black and M. S. Mathews), pp. 1100–1153. University of Arizona Press.

Hillgren V. J. and Boehler R. (1998) The light element in the core and core-mantle interactions (abstract). In *Origin of the Earth and Moon*, p. 10. LPI contribution 957. Lunar and Planetary Institute, Houston.

Hillgren V. J. and Boehler R. (1999) A case against Si as the light element in the Earth's core. *Lunar Planet. Sci.* **30**. Abstract No. 1650.

Hultgren R., Desai P. D. Hawkins D. T., Gleiser M., and Kelley K. K. (1973) In *Selected Values of the Thermodynamic Properties of Binary Alloys.* American Society for Metals. Metals Park, OH.

Ito E. and Katsura T. (1991) Dissolution of silicon and oxygen in molten iron at high pressure and temperature. *Proc. Jpn. Acad. Ser. B*67, 153–158.

Ito E., Morooka K., Ujike O., and Katsura T. (1995) Reaction between molten iron and silicate melts at high pressure: Implications for the chemical evolution of the Earth's core. *J. Geophys. Res.* 100B4, 5901–5910.

Javoy M. (1995) The integral enstatite chondrite model of the Earth. *Geophys. Res. Lett.* 22, 2219–2222.

Kilburn M. R. and Wood B. J. (1997) Metal-silicate partitioning and the incompatibility of S and Si during core formation. *Earth Planet. Sci. Lett.* 152, 139–148.

Knittle E. and Jeanloz R. (1989) Simulating the core-mantle boundary: An experimental study of high-pressures reactions between silicates and liquid iron. *Geophy. Res. Lett.* 16, 609–612.

Kokubo E. and Ida S. (2000) Formation of protoplanets from planetesimals in the solar nebula. *Icarus* 143, 15–27.

Lacaze J. and Sundman B. (1991) An assessment of the Fe-C-Si system. *Metall. Trans. A* 22A, 2211–2223.

Li J. and Agee C. B. (1996) Geochemistry of mantle-core differentiation at high pressure. *Nature* 381, 686–689.

Li J and Agee C. B. (2001a) The effect of pressure, temperature, oxygen fugacity and composition of nickel and cobalt between liquid Fe-Ni-S alloy and liquid silicate: Implications for the Earth's core formation. *Geochim. Cosmochim. Acta* 65, 1821–1832.

Li J. and Agee C. B. (2001b) Element partitionning constraints on the light element composition of the Earth's core. *Geophys. Res. Lett.* 28, 81–84.

Lin J-F., Heinz D. L., Campbell A. J., Devine J. M., Mao W. L., and Shen G. (2002) Iron-nickel alloy in the Earth's core. *Geophy. Res. Lett.* 29, 609–612.

Matas J., Ricard Y., Lemelle L., and Guyot F. (2000) An improved thermodynamic model of metal-olivine-pyroxene stability domains. *Contrib. Mineral. Petrol.* 140, 73–83.

O'Neill H. St. C., Canil D., and Rubie D. C. (1998) Oxide-metal equilibria to 2500°C and 25 GPa: Implications for core formation and the light component in the Earth's core. *J. Geophys. Res.* **103,** 12.,239–12,260.

Othani E., Yurimoto H., and Seto S. (1997) Element partitioning between metallic liquid, silicate liquid, and lower-mantle minerals: Implications for core formation of the Earth. *Phys. Earth Planet. Int.* 100, 97–114.

Poirier J. P. (1991) *Introduction to Physics of the Earth's Interior*. Cambridge University Press.

Poirier J. P. (1994) Light elements in the Earth's outer core: A critical review. *Phys. Earth Planet. Int.* 85, 319–337.

Righter K., Drake M. J., and Yaxley G. (1997) Prediction of siderophile element metal-silicate partition coefficient to 20 GPa and 2800°C: The effect of pressure, temperature, fO_2 and silicate and metallic melt composition. *Phys. Earth Planet. Int.* 100, 115–134.

Ringwood A. E. (1979) *Origin of the Earth and Moon*. Springer-Verlag.

Ringwood A. E. (1984) The Earth's core: Its composition, formation and bearing upon the origin of the Earth. *Proc. R. Soc. Ser. A* 395, 1–46.

Ringwood A. E. and Hibberson W. (1991) Solubilities of mantle oxides in molten iron at high pressure and temperatures: Implications for the composition of the Earth's core. *Earth Planet. Sci. Lett.* 102, 235–251.

Robie R. A., Hemingway B. S., and Fisher J. R. (1979) Thermodynamic properties of minerals and related substances at 298.15 K and 1 bar (10^5 Pa) pressure and at higher temperatures. Bulletin 1452. U.S. Geological Survey.

Rubie D. C. (1999) Characterising the sample environment in multianvil high-pressure experiments. *Phase Transitions* 68, 431–451.

Schlesinger M. E. and Xiang Q. (2001) Enthalpies of mixing in Fe-C-Si melts. *J. Alloys Compounds* 321, 242–247.

Thibault Y. and Walter M. (1995) The influence of pressure and temperature on the metal-silicate partition coefficients of nickel and cobalt in a model C1 chondrite and implications for metal segregation in a deep magma ocean. *Geochim. Cosmochim. Acta* 59, 991–1002.

Tronnes R. G. and Frost D. J. (2002) Peridotite melting and mineral-melt partitioning of major and minor elements at 22–24.5 GPa. *Earth Planet. Sci. Lett.* 197, 117–131.

Van Cappelen E. (1990) The parameterless correction method in X-ray microanalysis. *Microsc. Microanal. Microstruct.* **1,** 1–22.

Wänke H., Dreibus G., and Jagoutz E. (1984) *Mantle Chemistry and Accretion History of the Earth, Archean Geochemistry*. Springer-Verlag.

Wetherill G. H. (1994) Provenance of the terrestrial planets. *Geochim. Cosmochim. Acta* 58, 4513–4520.

Yang H. and Secco R. A. (1999) Melting boundary of Fe-17%Si up to 5.5 GPa and the timing of core formation. *Geophys. Res. Lett.* 26, 263–266.

Yoshino T., Walter M., and Katsura T. (2003) Core formation in planetesimals triggered by permeable flow. *Nature* 422, 154–157.